Vibrational modes of oxygen in GaP including second-nearest-neighbor interactions

R. J. Hauenstein and T. C. McGill
California Institute of Technology, Pasadena, California 91125

R. M. Feenstra
IBM, Thomas J. Watson Research Center, Yorktown Heights, New York 10598

(Received 11 October 1983)

The localized and resonant vibrational modes of a substitutional oxygen defect in GaP have been computed with the use of the Green's-function approach. A 15-parameter version of the deformable-dipole model was used to describe the lattice dynamics of bulk GaP. A defect, consisting of a mass perturbation at the substitutional site and a perturbation among the nearest- and second-nearest-neighbor short-range interactions near the oxygen atom, was considered. The local modes, labeled by symmetry, are presented as a function of the interaction perturbation. Quantitative agreement with experimental results for O^0 and O^+ defects is obtained by weakening the O (-Ga and -P) *short-range* interactions to 38% of the bulk values while *weakening* the Ga-P back bonds. With the inclusion of Coulomb effects, this corresponds to an effective O-lattice force constant of 3.5 eV/Å^2, which is 25% of the bulk, P-lattice value.

I. INTRODUCTION

The properties of the point defect GaP:O_P in which oxygen substituting for phosphorous in GaP forms a deep donor, have been actively studied, often generating considerable controversy.[1–6] In particular, numerous optical spectra have been reported. These highly structured spectra contain features due to transitions assisted by local phonons. By calculating the local vibrational modes of the O defect, we can, through comparison with the observed spectra, directly identify mode symmetries and characterize the atomic motion near the defect. We can also determine how the short-range interactions between atoms near the defect site are modified when the defect is introduced. In addition, assumptions of defect-site geometry (T_d symmetry and small local lattice relaxation, in particular) implicit in the local-mode calculation provide consistency checks on the interpretation of experimental results.

In this paper, we use the Green's-function approach to calculate the local phonon modes for oxygen isotopes on a phosphorous site in GaP. This work represents an extension of an earlier Green's-function calculation[7] in which bulk interactions were limited to nearest-neighbor (NN) interactions. Here, we use the deformable-bond approximation (DBA) of Kunc *et al.*[8] as the phenomenological description of bulk GaP. This 15-parameter model includes short-range interactions out to second-nearest neighbors (2NN) and long-range Coulomb effects arising from the electrostatic interaction between induced dipoles.[8] Our defect consists of a mass perturbation at the substitutional site and a perturbation in the short-range interactions among the 17-atom cluster consisting of the O, the four neighboring Ga, and the 12 2NN P atoms. We do not explicitly consider perturbations in the Coulomb interactions since their long range would render the Green's-function approach intractable. As we shall see, however, the Coulomb portion of the total interaction is relatively small and can be effectively contained in the short-range defect perturbation for sufficiently localized modes.

The DBA and Green's-function theory are briefly described in Sec. II. In that section we also discuss the defect perturbation considered in this work, and we derive an exact expression for the Coulomb contribution to the restoring force resulting from the displacement of a single atom in an infinite lattice. We find the Coulomb portion of the restoring force for a P-site single-atom displacement to be -17.7% of the bulk short-range component. Next, in Sec. III, we present our computed dispersion curves, density of states (DOS), and selected Green's functions for bulk GaP. In Sec. III we also present the results of our local-mode calculations for GaP:O_P. (Here, we shall use "local mode" to refer to both strictly localized and resonant modes, as in Ref. 7.) The interaction perturbation considered consists of varying certain O-Ga, O-P, and Ga-P (back-bond) force constants by the respective fractions, η, η, and 0.12η, of the corresponding bulk short-range values. Energies for local modes of a given symmetry are then presented as a function of the parameter η. The local DOS (LDOS) and "eigenvectors" are presented for selected local modes, and a discussion of the major features and the choice of defect parameters is given.

An extensive comparison to available photoluminescence data is made in Sec. IV. There, we see that the electron-capture luminescence data for the O^0 defect[2] is well described by our calculations for the value $\eta=-0.62$. In particular, we identify the phonon replicas at 24.7 and 28.4 meV with the peaks in our T_2 LDOS at 25.0 and 28.2 meV, respectively. Both peaks in the LDOS shift under isotopic substitution of ^{18}O for ^{16}O as expected. Our computed A_1 modes at 20.4 and 48.2 meV are observed for the charge states O^+ and O^0.[1,3] In all cases we

find substantial improvement in the agreement, both qualitative and quantitative, between calculated and observed values over that predicted by our earlier model.[7] Finally, the conclusions that can be drawn from this work are summarized in Sec. V.

II. COMPUTATIONAL METHOD

A. Bulk phonons

To describe the lattice dynamics of bulk GaP we have used the DBA. This model is a 15-parameter version of the deformable-dipole model of Kunc *et al.*, and has been shown to provide a good description of several III-V compounds.[8] The quantities of interest for our calculations are the force-constant matrix $\underline{\Phi}$ and the dynamical matrix $\underline{D}$, which is related to $\underline{\Phi}$ by the equation, $\underline{D}=\underline{M}^{-1/2}\underline{\Phi}\underline{M}^{-1/2}$. In this expression, $\underline{M}$ is a diagonal matrix whose elements are equal to the masses in the problem. In the DBA, the force-constant matrix has the form

$$\underline{\Phi}=\underline{\Phi}^{(\mathrm{SR})}+\underline{\Phi}^{(\mathrm{el})} ,$$
$$-\underline{\Phi}^{(\mathrm{el})}=(\underline{Z}+\underline{N}^{\dagger})(\mathbb{1}-\underline{B}\,\underline{a})^{-1}\underline{B}(\underline{Z}+\underline{N}) , \tag{1}$$

where $\underline{\Phi}^{(\mathrm{SR})}$ and $\underline{\Phi}^{(\mathrm{el})}$ correspond, respectively, to the short-range and electrostatic terms. The short-range force-constant matrix $\underline{\Phi}^{(\mathrm{SR})}$ contains the non-Coulombic interactions which in the DBA extend out to 2NN's. As a consequence of the T_d^2 symmetry of GaP, the off-diagonal Cartesian blocks can be shown to have the form[8]

$$\underline{\Phi}^{(\mathrm{SR})}(\mathrm{Ga;P})=\underline{\Phi}^{(\mathrm{SR})}(\mathrm{P;Ga})=\begin{bmatrix} A & B & B \\ B & A & B \\ B & B & A \end{bmatrix} , \tag{2a}$$

$$\underline{\Phi}^{(\mathrm{SR})}(\mathrm{Ga;Ga})=\begin{bmatrix} C_1 & D_1 & E_1 \\ D_1 & C_1 & E_1 \\ -E_1 & -E_1 & F_1 \end{bmatrix} , \tag{2b}$$

and

$$\underline{\Phi}^{(\mathrm{SR})}(\mathrm{P;P})=\begin{bmatrix} C_2 & D_2 & -E_2 \\ D_2 & C_2 & -E_2 \\ E_2 & E_2 & F_2 \end{bmatrix} , \tag{2c}$$

for interactions between NN's [Eq. (2a)] and 2NN's [Eqs. (2b) and (2c)], respectively. These Cartesian blocks must obey the transformation law[9]

$$\Phi_{\alpha\beta}(L,K;L',K')=\sum_{\mu,\nu} S_{\alpha\mu}S_{\beta\nu}\Phi_{\mu\nu}(l,\kappa;l',\kappa') , \tag{3}$$

where $\underline{S}$ is the point-group operation associated with the space-group transformation which takes the site (l,κ) into the site (l',κ'). In this expression, l, l', L, and L' label the N unit cells in the lattice, κ, κ', K, and K' specify the basis atom, and the remaining indices refer to Cartesian coordinates. Hence, from Eqs. (2), (3), and the translation-invariance condition,[9]

$$\underline{\Phi}(l,\kappa;l,\kappa)=-\sum_{l',\kappa'\neq l,\kappa}{}' \underline{\Phi}(l,\kappa;l',\kappa') , \tag{4}$$

$\underline{\Phi}^{(\mathrm{SR})}$ for the entire lattice is determined. The description of the bulk short-range interaction in terms of these 10 parameters $(A-F_2)$ is the most general description allowed by symmetry, and it physically corresponds to both central and noncentral pair interactions.[8]

In addition to purely short-range forces, the DBA force-constant matrix contains a contribution from classical electrostatic interactions. Associated with each lattice site is an effective charge $\underline{Z}$. Displacement of a charge from its equilibrium site effectively results in an electric dipole moment at the site. Dipoles may also be *induced*, either by the motion of neighboring atoms (mechanical polarizability $\underline{N}$) or by the electric fields produced by other dipoles (electronic polarizability $\underline{a}$). The dipoles, however generated, produce electric fields. These fields exert forces on the charges and mechanically induced dipoles, giving rise to the Coulomb term $\underline{\Phi}^{(\mathrm{el})}$ of Eq. (1). Five parameters are used to determine $\underline{\Phi}^{(\mathrm{el})}$, giving a total of 15 for the DBA.[8] These 15 parameters have been determined for GaP by Kunc *et al.*[8]

B. Green's functions and group-theoretic considerations

The bulk Green's functions are numerically obtained from the eigenvalues and eigenvectors of the Fourier-transformed dynamical matrix in precisely the manner described in Ref. 7. From the bulk Green's functions the standard formalism[10] is used to obtain the local modes as before.[7] The major difference in the present work lies in the spatial extent of the defect considered. Here, the defect affects 17 atoms and, hence, 51 Cartesian coordinates. Thus, we are required to evaluate a 51×51 block of the bulk Green's-function matrix.[10]

We shall consider substitutional defects which retain the full point-group symmetry (T_d) of the lattice. Accordingly, it is natural and convenient to express the Green's-function matrix in a basis of "collective coordinates" which transform according to the irreducible representations of T_d. It can be readily shown that the 51-dimensional *reducible* representation Γ of T_d given in terms of Cartesian coordinates can be reduced to

$$\Gamma=3A_1\oplus A_2\oplus 4E\oplus 5T_1\oplus 8T_2 . \tag{5}$$

The collective coordinates Q transforming according to the irreducible representations (A_1-T_2), are related to the original Cartesian coordinates by an orthogonal transformation. The collective coordinates have already been determined for the five-atom cluster.[7] The additional collective coordinates needed for the 12-atom, 2NN shell are given in the Appendix.

The advantage of the collective-coordinate transformation is that matrices reflecting the T_d symmetry are block-diagonalized in the form[7,9]

$$G^{0(s)(r)}_{\mu\nu;\sigma\rho}=\delta_{(s)(r)}\delta_{\mu\nu}G^{0(s)}_{\sigma\rho} , \tag{6}$$

where (s) and (r) label the irreducible representation. The block diagonalization allows us to consider each irreducible representation separately, providing a classification

scheme for the defect vibrational motion according to symmetry. For a given irreducible representation, μ and ν label the dimension, and σ and ρ label the occurrences (e.g., $\mu=1,2,3$ and $\sigma=1,\ldots,8$ for T_2). The form of the block diagonalization also restricts the number of independent matrix elements on the basis of symmetry. With the use of Eq. (6), the number of independent Green's-function matrix elements is reduced to 68.

C. Defect perturbation

The defect perturbation considered in this work consists of the mass substitution $m_P \rightarrow m_O$ at the defect site and a perturbation of the short-range force constants among the substituent and its NN's and 2NN's. We wish to consider a general force-constant perturbation $\delta\underline{\Phi}$ having the block form of Eq. (2) and consistent with T_d symmetry. Let us label the O-Ga perturbation parameters δA and δB, the O-P parameters $\delta C,\ldots,\delta F$, the Ga-P NN back-bond parameters $\delta A'$ and $\delta B'$, the intra-Ga-shell 2NN parameters $\delta C',\ldots,\delta F'$, and the intra-P-shell 2NN parameters $\delta C'',\ldots,\delta F''$. Now, not all these force-constant parameters may be chosen independently. Applying the infinitesimal-rotation-invariance condition,[9] we find that

$$\delta E=\delta E'=\delta E''=0\ , \tag{7a}$$

$$\delta A'-\delta B'=0\ , \tag{7b}$$

$$\delta A-\delta B=-2[(\delta C'-\delta D')+\delta F']\ , \tag{7c}$$

$$\delta F=-2(\delta C''-\delta D'')\ , \tag{7d}$$

$$2\,\delta F''=-(\delta C-\delta D)\ . \tag{7e}$$

The linear combinations of the form $\delta A-\delta B$ represent NN bond-bending spring constants.[7] Similarly, $\delta C-\delta D$, δF, and the corresponding primed expressions may be viewed as *anisotropic* bond-bending springs between 2NN pairs, while the parameters δE correspond to a more complicated pair interaction. Essentially, Eqs. (7) impose constraints on the noncentral pair interactions possible within an *isolated* cluster having the geometry of our 17-atom defect. The results up to this point (given our above assumptions) are general, leaving nine free quantities to specify $\delta\underline{\Phi}$.

We are now ready to parametrize the interaction perturbation. To reduce the number of free parameters, we assume the same fractional variation among *independent* O-Ga, O-P, and Ga-P parameters, giving

$$\delta A/A=\delta B/B=\eta_{O,Ga}\ , \tag{8a}$$

$$\delta C/C_2=\delta D/D_2=\delta F/F_2=\eta_{O,P}\ , \tag{8b}$$

$$\delta A'/A=\eta_{Ga,P}\ . \tag{8c}$$

If we make the analogous assumptions, $\delta C'/C_1=\delta D'/D_1=\delta F'/F_1$ and $\delta C''/C_2=\delta D''/D_2$, we see from Eqs. (7) that the interaction perturbation $\delta\underline{\Phi}$ is completely specified in terms of the η's. In this way, we specify directly the NN ($\eta_{O,Ga}$), the adjustable part of the 2NN ($\eta_{O,P}$), and the bond-stretching part, $\delta A'+2\delta B'=3\delta A'$, of the back-bond interactions ($\eta_{Ga,P}$). Other interactions within the cluster are then modified automatically according to rotation invariance.

The defect-perturbation matrix is now

$$\delta\underline{L}=\underline{M}^{-1/2}\delta\underline{\Phi}\,\underline{M}^{-1/2}-\omega^2\underline{M}^{-1}\delta\underline{M}\ ,$$

where $\delta\underline{M}$ contains the on-site mass perturbation. (Note that we have put the explicit mass dependence in $\delta\underline{L}$ rather than $\underline{G}^0$, as in Ref. 7.) We numerically construct $\delta\underline{L}$ in Cartesian form, using Eqs. (2)–(4), (7), and (8), and then apply the transformation to collective coordinates. The local modes are given by the frequencies ω which solve[10]

$$\mathrm{Re}\det[\underline{1}-\underline{G}^0(\omega^2)\delta\underline{L}(\omega^2)]=0\ . \tag{9}$$

We solve such a determinantal equation for each irreducible representation. A useful quantity for characterizing the relative amount of motion of a certain symmetry type and at a particular frequency is the LDOS. The LDOS of the perturbed crystal is given by the diagonal elements of $-\mathrm{Im}\underline{G}/\pi$, where the perturbed crystal Green's function is given by[10]

$$\underline{G}=(\underline{1}-\underline{G}^0\delta\underline{L})^{-1}\underline{G}^0\ . \tag{10}$$

Strong resonant modes show up ideally as Lorentzian peaks in the LDOS while strictly localized modes appear as δ functions.[7] For representations which have multiple occurrences in the space of the defect, the LDOS for each occurrence provides a measure of the fraction of total kinetic energy in that particular type of motion, and this quantity is used in the following sections to describe the composition of defect modes.

D. Restoring force for one-atom displacements

In the discussion to follow, it will be useful to know the effective spring constant acting on the O atom under a unit displacement from equilibrium. This spring constant is given by $k^{(\mathrm{eff})}=k'^{(\mathrm{SR})}+k^{(\mathrm{el})}$, where

$$k'^{(\mathrm{SR})}=-4[(A+\delta A)+2(C_2+\delta C)+(F_2+\delta F)] \tag{11}$$

denotes the modified short-range part, and $k^{(\mathrm{el})}$ is the bulk P-site Coulomb component. We wish to compute $k^{(\mathrm{el})}$. In the notation of Maradudin,[9] we have for the unit displacement $u_\beta(l',\kappa')=\delta_{\alpha\beta}\delta_{ll'}\delta_{\kappa\kappa'}$,

$$\begin{aligned}F_\alpha(l,\kappa)&=-\sum_{\beta,l',\kappa'}\Phi_{\alpha\beta}(l,\kappa;l',\kappa')\delta_{\alpha\beta}\delta_{ll'}\delta_{\kappa\kappa'}\\&=-\Phi_{\alpha\alpha}(l,\kappa;l,\kappa)\ ,\end{aligned} \tag{12}$$

where $\Phi_{\alpha\alpha}(l,\kappa;l,\kappa)=k^{(\mathrm{el})}$ for $\underline{\Phi}=\underline{\Phi}^{(\mathrm{el})}$. Now, using the identity

$$\delta_{ll'}=\frac{1}{N}\sum_{\vec{k}}\exp\{-i\vec{k}\cdot[\vec{x}(l,\kappa)-\vec{x}(l',\kappa)]\} \tag{13}$$

in Eq. (12) gives

$$\begin{aligned}F_\alpha(l,\kappa)&=-\frac{1}{N}\sum_{\vec{k}}\Big[\sum_{l'}\Phi_{\alpha\alpha}(l,\kappa;l',\kappa)\\&\qquad\times\exp\{-i\vec{k}\cdot[\vec{x}(l,\kappa)-\vec{x}(l',\kappa)]\}\Big]\\&=-\frac{1}{N}\sum_{\vec{k}}\hat{\Phi}_{\alpha\alpha}(\kappa,\kappa\,|\,\vec{k})\ ,\end{aligned} \tag{14}$$

where the inner sum has been identified as the Fourier-transformed force-constant matrix. Recognizing that our $\hat{\Phi}(\kappa,\kappa \mid \vec{k})$ transforms as $T_2 \otimes T_2$, we can restrict the summation over $\vec{k}$ in Eq. (14) to the irreducible wedge W of the first Brillouin zone as in Ref. 7, obtaining finally

$$k^{(\mathrm{el})} = \frac{1}{N} \sum_{\vec{k} \in W} h_{\vec{k}} \sum_{\beta=1}^{3} \mathrm{Re}[\hat{\Phi}^{(\mathrm{el})}_{\beta\beta}(\kappa,\kappa \mid \vec{k})] \, . \tag{15}$$

This sum was evaluated numerically by a method similar to the numerical computation of $\mathrm{Im}\underline{G}^0$ in this and in our previous work.[7] The result is $k^{(\mathrm{el})} = -0.177 k^{(\mathrm{SR})}$ for the bulk P site.

III. RESULTS

A. Bulk phonons

In Fig. 1 we show the bulk dispersion curves and bulk DOS for GaP as computed from the DBA. The DBA results constitute a substantial quantitative improvement over those of the two-parameter model used previously.[7] The calculated LO_Γ and TO_Γ energies, 50.0 and 45.3 meV, respectively, are split due to Coulomb effects and are in agreement with measured values.[8] The calculated TA_X energy is 12.8 meV compared with the actual value, 13.1 meV.[11] The bulk DOS presented here is highly structured compared with that of the two-parameter model.[7] As we shall see, this structure gives rise to local-mode behavior not seen in the simpler model. In the units shown in the figure, the computed area under the bulk-DOS curve is 6.0004, compared to the exact theoretical value, 6.

B. Bulk Green's functions

We have computed the bulk Green's-function matrix $\underline{G}^0$ for both a P-centered and a Ga-centered 17-atom cluster. The method of computation is described in Ref. 7. The Green's functions were calculated as functions of $(\hbar\omega)^2$ at intervals of 2.5 meV^2 and then converted to functions of $E = \hbar\omega$ [see Eq. (9) of Ref. 7]. This corresponds to a resolution in E of about 0.5 meV near $E = 0$ and 0.025 meV at $E = 50$ meV. There are 68 bulk Green's functions each for both the P- and Ga-centered clusters—too many to display individually. Instead, for each irreducible representation (s), we sum the diagonal matrix elements and present $\mathscr{D}^{(s)}(E)$ vs E in Fig. 2, where

$$\mathscr{D}^{(s)}(E) \equiv -\frac{1}{\pi} \mathrm{Tr}\,\mathrm{Im}[\underline{G}^{0(s)}(E)] \, . \tag{16}$$

The quantity $\mathscr{D}^{(s)}(E)$ is the partial DOS (Ref. 7) for the representation (s) and is proportional to the mean-squared amplitude of modes associated with (s)-type motion in the 17-atom cluster at energy E. In particular, the A_2 mode consists of 2NN motion only. From Fig. 2 we see that the P-centered, A_2 partial DOS has a large amplitude in the TO and small amplitude in the TA phonon branches, while the opposite is true for the Ga-centered DOS. This is because the P atoms undergo larger displacements in optical modes than do the heavier Ga atoms. For the discussion to follow, the important symmetries are A_1 and T_2. A_1 modes consist of some combination of the following: "breathing" motion of the NN shell, 2NN breathing, and a third, more complicated 2NN motion. T_2 modes consist of defect-site motion along with collective motions within the NN and the 2NN shells. Only T_2 modes can involve defect-site motion. (See the Appendixes here and in Ref. 7 for a complete listing of the collective coordi-

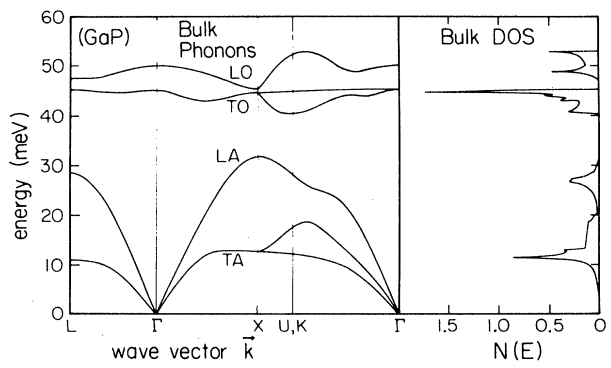

FIG. 1. Bulk-phonon dispersion curves and DOS for GaP calculated from the DBA. The calculated LO_Γ, TO_Γ, and TA_X energies are 50, 45.3, and 12.8 meV, respectively. The peaks in the bulk DOS lie at 11.3, 27, 44.8, 48.8, and 52.9 meV. In the units shown, the DOS integrates to 6.0004, compared with the exact value, 6.

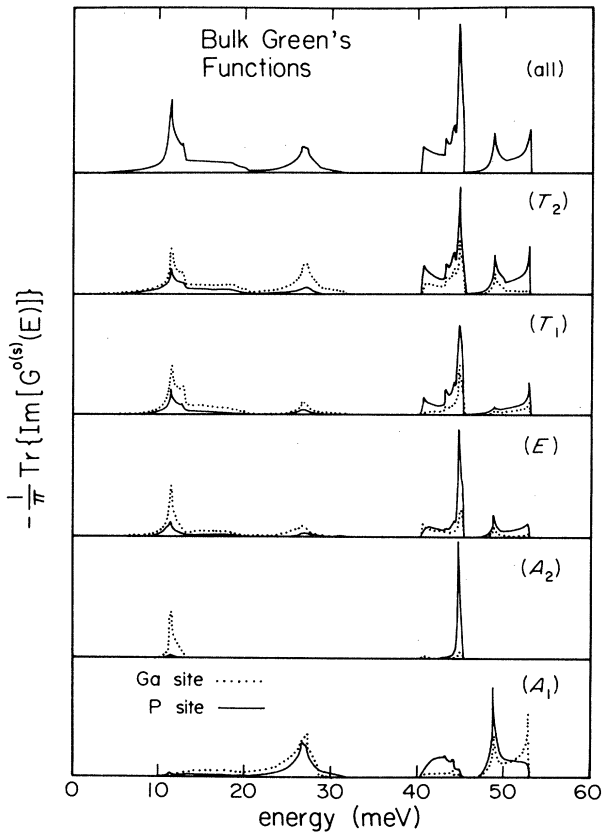

FIG. 2. Partial DOS of bulk GaP for the representations, A_1–T_2. Green's functions for P- and Ga-centered clusters are shown. The A_2 partial DOS involves 2NN motion only and for the P-centered (Ga-centered) cluster is larger at optical (acoustic) frequencies.

nates of the 17-atom cluster.)

Figure 2 gives the decomposition of the bulk DOS into the various representations of T_d appropriate for a point defect. The bulk DOS can be recovered from the various partial densities by performing the sum

$$\sum_{(s)=A_1}^{T_2} d_{(s)}[\mathscr{D}_{\mathrm{P}}^{(s)}(E)+\mathscr{D}_{\mathrm{Ga}}^{(s)}(E)]=17N(E)\ , \qquad (17)$$

where $d_{(s)}$ is the dimensionality of the representation (s). The renormalization factor of 17 on the right-hand side of Eq. (17) occurs because, in summing over both P- and Ga-centered clusters, the two-atom basis of GaP is included 17 times.

C. Local modes

Let us examine the local phonon modes of GaP:O_P as a function of the interaction perturbation. In Sec. II C we have parametrized the interaction perturbation for GaP:O_P in terms of $\eta_{O,Ga}$, $\eta_{O,P}$, and $\eta_{Ga,P}$. Now, we feel physically motivated to require a further constraint between $\eta_{O,Ga}$ and $\eta_{O,P}$. It is natural to expect the O-P interaction to vanish when the O-Ga interaction vanishes, and the O-P interaction to have the bulk (P-P) value when the O-Ga interaction has the bulk (P-Ga) value. In this way we are led to consider defects for which $\eta_{O,Ga}=\eta_{O,P}=\eta$. In contrast, we expect the relation between the back bonds ($\eta_{Ga,P}$) and our newly defined η to depend on details of the defect chemistry well beyond the scope of this paper. In practice, we have found that the effect of the parameter $\eta_{Ga,P}$ is to "turn on" certain 2NN-shell local modes while not appreciably affecting those low-shell modes which have a strong dependence on η. Therefore, for the purpose of presentation, we *choose* (see Sec. IV) $\eta_{Ga,P}=0.12\eta$ and present our results as a function of the single parameter, η.

The local modes of GaP:O_P as a function of the perturbing force-constant parameter η are shown in Fig. 3. Only A_1 and T_2 modes satisfying Eq. (9) are shown here. Modes of A_2, E, and T_1 symmetry also occur, but are omitted for clarity. η ranges from -1, corresponding to removal of the *short-range* O-Ga and O-P interactions, through 0, where all interactions have their bulk values, to $+1$. The effective O-site restoring force, $k^{(\mathrm{eff})}=(1+\eta-0.177)/(1-0.177)$, normalized to the bulk P-site value, is indicated along the top of the figure while the bulk DOS adjoins on the left. Note that the shaded region below the value $k^{(\mathrm{eff})}=0$ is unphysical.

The important features of Fig. 3 are the steep T_2 branch in the energy range near 12–40 meV, the lowest-lying T_2 branches (around 10 meV), the low-energy A_1 branch (20–35 meV), and the high-energy A_1 branch (45–55 meV). The steep T_2 branch was seen in our earlier model[7] and consists mainly of O-atom motion. Also seen in our earlier work was the low-energy A_1 branch. In the present work, this A_1 branch, consisting of over 95% NN breathing, has been pulled up to higher energies ($\eta<0$) in better agreement with experiment, as we shall see below. Two significant features appear in the present work not obtained previously. One is the high-energy A_1 branch, which appears only upon perturbation of the Ga-P back-bond force constants and involves mostly 2NN-breathing motion. The other is the low-energy T_2 branch. This T_2 branch is primarily composed of Ga-shell, bond-stretching motion ($E\gtrsim 6$ meV) and seems to appear for $\eta<0$ only when the bulk model includes 2NN interactions.

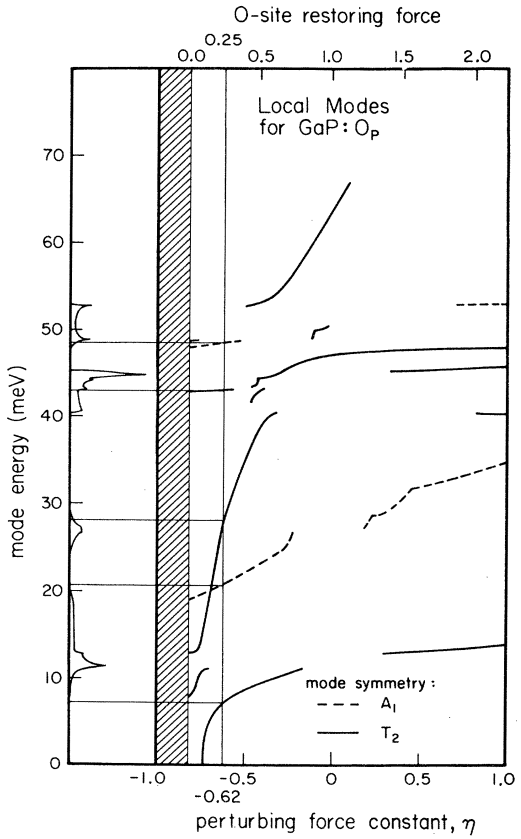

FIG. 3. A_1 and T_2 local-mode energies for GaP:O_P as a function of the short-range force-constant perturbation η discussed in the text. For $\eta=-0.62$ the A_1-mode energies are 20.4 and 48.2 meV and the T_2-mode energies are 7.3, 28.2, and 43.1 meV. The shaded region is unphysical. The DOS for bulk GaP adjoins on the left.

In Sec. IV we shall see that the O^0 defect is well described by the perturbation $\eta=-0.62$. This corresponds to a $k^{(\mathrm{eff})}$ of 25% of the bulk value. The local-mode energies at $\eta=-0.62$ are indicated in the caption of Fig. 3. Next, in Fig. 4, we compare the A_1 bulk and defect partial DOS for $\eta=-0.62$. These are decomposed into their Ga- and P-shell parts, showing the relative energy of motion associated with each shell at a given mode "energy," $E=\hbar\omega$. From the top curve in Fig. 4 we see resonant modes at 20.4 and 48.2 meV. The 20.4-meV mode is a rather broad resonance of width ~ 5 meV and involves mainly NN Ga motion (96%) as mentioned above. The resonant mode at 48.2 meV is sharper (~ 0.5 meV) and consists of motion (97%) of the less massive P atoms. It is evident from the figure that both resonant modes occur at frequencies appreciably different from the bulk peaks, and hence are characteristic of the defect. In contrast, local modes confined near singular features in

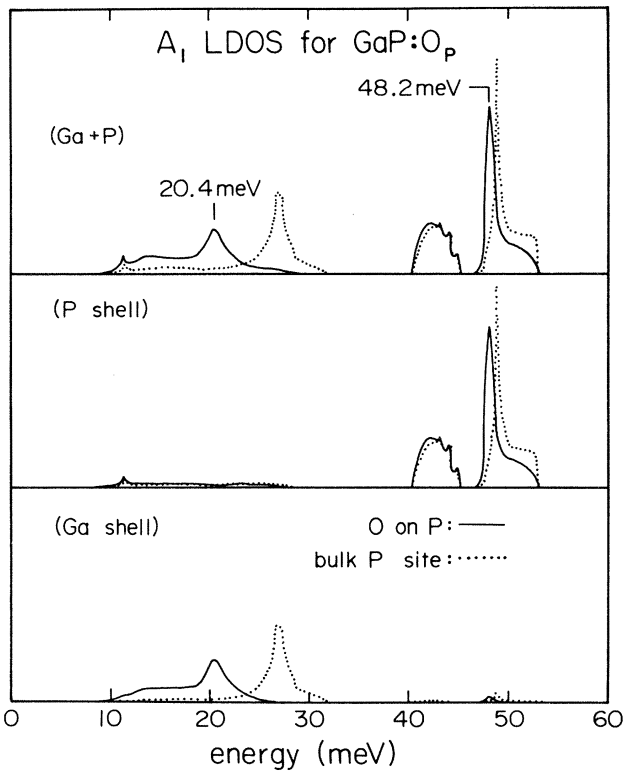

FIG. 4. A_1 LDOS for GaP:O_P decomposed into Ga- and P-shell components. The corresponding bulk partial DOS's are included for comparison. The 20.4-meV resonance involves mostly Ga-shell motion, while the resonance at 48.2 meV consists mainly of P-shell motion. All curves have the same scale.

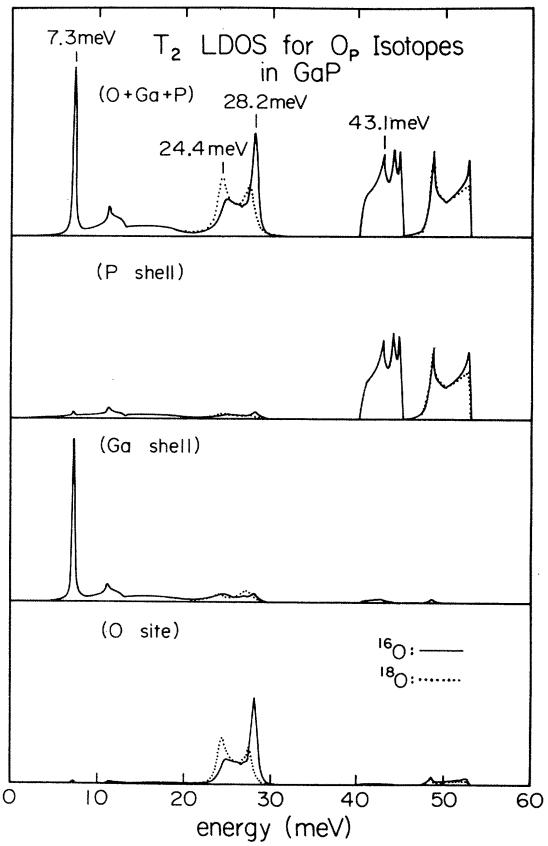

FIG. 5. T_2 LDOS of Ga:O_P for isotopes ^{16}O and ^{18}O decomposed into O-atom, NN-shell, and 2NN-shell parts. The twin resonances centered near 25 meV primarily involve O-atom motion and undergo isotope shifts. Other resonant modes occur at 7.3 meV (Ga shell) and 43.1 meV (bulklike P shell). All curves have the same scale.

the bulk partial DOS may also, in general, occur. Such modes evidently couple strongly to bulk modes and are thereby more "bulklike," i.e., more spatially delocalized in character.

We show the T_2 LDOS for GaP:O_P at $\eta=-0.62$ in Fig. 5, once again decomposed into contributions from O, Ga, and P shells. The mode energies which solve Eq. (9) are indicated on the top curve. Twin resonance peaks at 25.0 and 28.2 meV are seen in the O-site LDOS, occurring just above and just below the 27-meV LA peak in the bulk DOS. The 28.2-meV mode consists of 86% O-, 8% Ga-, and 6% P-shell motion, and the 25.0-meV mode consists of 70% O-, 20% Ga-, and 10% P-shell motion, within the 17-atom cluster. We note that at $\eta=-0.62$ only the mode at 28.2 meV is a solution of Eq. (9). The twin-peak structure appears to be the result of coupling between isolated-defect and nearby bulk LA-phonon modes. The 27-meV LA peak in the bulk DOS involves very little P-sublattice motion. Thus, a mode involving large O motion cannot exist at 27 meV, and when $\eta\rightarrow-0.62$ the O mode splits into two modes. Both O-site peaks occur at energies different from bulk peaks and are well localized near the O atom, and upon the substitution of ^{18}O for ^{16}O, both peak positions undergo a shift in energy. The 25.0- and 28.2-meV resonances are, therefore, local rather than bulklike in character. In contrast, the weak mode at 43.1 meV is pinned to a van Hove singularity in the bulk DOS (see Fig. 3) and is evidently somewhat more bulklike. Finally, the sharp resonance at 7.3 meV primarily involves Ga-shell motion (94%) along with small P (5%) and O (1%) contributions.

IV. DISCUSSION

A. Intensity of phonon replicas

The intensity of phonon-assisted optical transitions at defects have been thoroughly discussed by Rebane.[12] Selection rules for determining which transitions are allowed are similar to those used for molecules, as discussed by Herzberg.[13] Allowed transitions are those for which the dipole matrix element

$$\langle \Psi_m(r,R)\Phi_{mj}(R) \mid D_e(r) \mid \Psi_l(r,R)\Phi_{li}(R) \rangle$$

is nonzero. Here, Ψ is the electronic wave function, Φ is the vibrational wave function, l and m label electronic states, i and j label vibrational states, r is the set of all electron coordinates, R is the set of all nuclear coordinates, and $D_e(r)=-e\sum_i r_i$ is the electronic dipole moment operator. In place of the nuclear coordinates R, we introduce new coordinates Q_{l_s} which are the normal coor-

dinates of the vibrational problem. These normal coordinates may be chosen to form bases for irreducible representations $\Gamma(Q_{l_s})$ of the symmetry group of the imperfect crystal, where $\Gamma(x)$ refers to the representation according to which x transforms. We assume that the same set of normal coordinates may be used for both the initial and final electronic states (though the equilibrium values of these coordinates will depend on the electronic state). The total vibrational wave function can now be written as

$$\Phi_{l\{i_s\}}=\prod_s \phi_{i_s}(Q_s)\ , \tag{18}$$

where i_s labels the occupation of the sth normal coordinate. The harmonic-oscillator functions ϕ are even with respect to their arguments for even occupation, and odd for odd occupation. By inspection, in the vibrational ground state ($i_s=0$ for all s) the wave function $\Phi_{l\{i_s\}}$ is totally symmetric. For multiple one-phonon occupation, Φ transforms as $\prod_{\{i_s=1\}}\Gamma(Q_s)$, where the product runs over all s such that $i_s=1$.

As an example of the above discussion, consider a defect with T_d symmetry, in which case the dipole moment transforms as T_2. An $A_1\rightarrow A_1$ electronic transition is forbidden, but if one T_2 phonon is involved, the dipole matrix element transforms as

$$A_1\otimes A_1\otimes T_2\otimes A_1\otimes T_2=A_1\oplus E\oplus T_1\oplus T_2\ ,$$

which is allowed. Similarly, an $A_1\rightarrow T_2$ electronic transition is allowed, and participation of a single A_1 phonon or a single T_2 phonon is also allowed since

$$A_1\otimes A_1\otimes T_2\otimes T_2\otimes A_1 \quad\text{and}\quad A_1\otimes A_1\otimes T_2\otimes T_2\otimes T_2$$

both contain A_1. The intensity of phonon replicas is governed by the Franck-Condon principle.[12,13] Essentially, this principle states that the phonon replicas which will be observed in a transition are those which describe the change in equilibrium position of the atoms between the initial and final states. In other words, if the atoms move along some coordinate Q between their initial and final states, normal modes of the type Q will be strongly excited in the transition.

We can use this principle to demonstrate that "antisymmetric," i.e., not totally symmetric, phonons cannot be strongly excited. If some antisymmetric vibrational mode is strongly excited, this necessarily leads to a change in the symmetry of the system, and in the new symmetry group the vibrational mode is totally symmetric. However, for weak excitation of the antisymmetric vibrations, this change in symmetry can be neglected. Thus, in electronically allowed transitions, totally symmetric vibrations will predominate, and in electronically forbidden transitions, the occupation of the dominant antisymmetric modes changes by one.

B. Comparison of theory and experiment

In Table I we compare our theoretical results with the phonon energies observed in the optical spectra of the O^+ and O^0 defects. The apparent agreement between theory and experiment is achieved partly by matching unknown theoretical parameters with experiment, and partly by the predictive powers of the theory itself. If we view the bulk phonon dispersion curves as input to the theory, then the only unknown is the interaction perturbation within the 17-atom cluster. We have parametrized the interaction perturbation [Eqs. (8)] in Sec. II C and have invoked the further restriction, $\eta_{O,Ga}=\eta_{O,P}=\eta$ in Sec. III C, so that the total number of unknown parameters is two. We determine values for these parameters by matching the en-

TABLE I. Energies (meV) of the phonons associated with the O^0 and O^+ defect in GaP. $^{16}O\rightarrow{}^{18}O$ isotope shifts (meV) are given in parentheses following the energies. Tentative identifications are indicated by "?."

Label	Expt.	Theory	Identification
Zn-O	6.0[a]	7.3	defect (T_2, Ga shell)
TA	13.1[b]	11.5	bulk (TA)
a_1(Ga)	19.5,[c] 19[d]	20.4	defect (A_1, Ga shell)
loc	24.7(−1.6)[b]	25.0(−0.6)	defect (T_2, O atom)
loc′	28.4−0.5)[b]	28.2(−0.7)	defect (T_2, O atom)
A	43.0[b]	43.1	defect (T_2, P shell)?
TO	44.8[b]	44.8	bulk (TO)
e(P)	· · ·	45.3	defect (E, P shell)
t_1(P)	· · ·	45.4	defect (T_1, P shell)
a_2(P)	· · ·	45.8	defect (A_2, P shell)
B	46.1,[b] 46.4,[c], 46.5[e]	48.8	defect (T_2, P shell)?
a_1(P)	47.5,[b] 47,[f] 48[d]	48.2	defect (A_1, P shell)
C	48.7,[b] 48.8[c]	48.8	bulk (LO)
LO_Γ	49.8[b]	50.0	bulk (LO_Γ)

[a] Reference 17.
[b] Reference 2, capture-luminescence spectrum.
[c] Reference 2, luminescence-excitation spectrum.
[d] Reference 3.
[e] Reference 14.
[f] Reference 1.

ergies of theoretical modes with those observed. The theory then predicts a number of other vibrational modes not involved in the matching process with which we identify observed phonons. In this way we determine the symmetry and character of almost all of the phonon modes associated with the O^+ and O^0 defects. Strictly speaking, all of the phonons observed in the optical spectra involve some component of defect motion (i.e., O-atom, nearest Ga-shell, or nearest P-shell motion). However, certain phonons involve much more defect motion than others, and it is useful to separate the modes into those which are associated largely with the defect and those which are bulklike. In Table I we have classified the modes as such. The theoretical defect-mode energies are taken from peaks in the LDOS, and the theoretical bulk phonon energies are taken from peaks in the bulk DOS or critical points in the dispersion curves.

A set of very interesting phonon sidebands associated with the neutral oxygen defect O^0 occur in the capture luminescence of Dean and Henry.[2] Here, intense phonon resonances near 25 meV are observed to involve significant O motion since they shift under the isotopic substitution, $^{16}O \rightarrow {}^{18}O$ and must therefore be T_2 modes. Since the O mass is less than that of P, these low-energy resonances imply reduced O-neighbor force constants relative to the bulk force constants. This force-constant reduction was first estimated by Feenstra and McGill[14] to be 30%, and later estimated by Baraff, Kane, and Schlüter[15] to be 20%; both estimates were based on simple molecular-type vibrational models. Subsequent NN Green's-function results[7] yield an estimate of 15%. In the present model, if we assume the same fractional reduction for O-Ga and O-P force constants, the best value for the purely short-range force-constant reduction is $\eta = -0.62$. After including Coulomb effects between the O atom and the rest of the lattice, this corresponds to a total effective force constant ($k^{(\text{eff})}$) of 3.5 eV/Å^2, which is 25% of the bulk, P-site value. We emphasize, though, that $k^{(\text{eff})}$ includes long-range Coulomb effects from the entire lattice and must *not* be viewed simply as an equivalent short-range force constant. Our LDOS for T_2 modes, summed over the O atom, Ga shell, and P shell, is shown in Fig. 5. The theoretical peak energies and isotope shifts listed in Table I compare reasonably well with experiment.

Having determined the O-neighbor force constants, the theory predicts an A_1 mode at 20.4 meV. We identify this mode with the observed 19-meV phonon listed in Table I. As discussed by Morgan[4] and also in Sec. IV A, the observed intensities of this 19-meV mode and the prominent 47-meV mode indicate that these modes have A_1 symmetry. To produce a defect mode of A_1 symmetry near 47 meV, it is necessary to reduce the back-bond Ga-P force constants from their bulk values. We arbitrarily choose to reduce the Ga-P force constants by 12% of the O-neighbor reduction, resulting in $\eta_{\text{Ga,P}} = -0.0744$ for the Ga-P interactions and yielding an A_1 mode at 48.2 meV. Further reductions in the Ga-P force constants reduce the energy of this mode, bringing it closer to the observed value. However, considering the uncertainties associated with our calculated optical phonons, we feel that an accurate determination of these back-bond Ga-P interactions is outside the range of our theory. Suffice it to say that our computations do yield an A_1 mode in the optical branch and that the back-bond Ga-P interactions are reduced from their bulk values.

A number of phonon replicas in the optical branch are seen in the optical spectra of Dean and Henry.[2] We identify the symmetry and nature of these phonons as indicated in Table I. Some of these optical-phonon replicas are weak, and considering the uncertainty of our optical-phonon computations, those identifications we feel should be regarded as tentative are marked by "?." The a_1(P) phonon has been discussed above. The phonon labeled *B* we take to be a defect mode since its energy falls well away from peaks in the bulk DOS. This phonon is observed in capture-luminescence and luminescence-excitation spectra,[2] and is also seen in the near-neighbor ($m = 4$ and 5) Zn-O pair spectrum[14] (labeled O in that spectrum). Considering the proximity of the donor-acceptor impurities in the latter case, it seems that this 46.5-meV mode corresponds to atomic motion which is directed along the donor-acceptor axis, i.e., a T_2 mode with respect to the T_d symmetry of an isolated O impurity. The 46.1-meV *B* phonon in the capture-luminescence spectrum most likely has T_2 symmetry,[4] although the 46.4-meV mode seen in luminescence-excitation spectra could transform as either A_1 or T_2, as discussed in Sec. IV A. For now, we group all three of these modes together with the label *B* in Table I, and we tentatively identify them with a computed T_2 resonance at 48.8 meV which is strongly tied to a LO peak in the bulk DOS (see Figs. 3 and 5).

Another T_2 defect mode occurs in the theory at 43.1 meV, and this mode we tentatively associate with the observed 43.0-meV phonon labeled *A*. The 49.8-meV phonon identified by Dean and Henry as LO_Γ is in agreement with our computed 50.0-meV LO_Γ-phonon energy. The mode labeled *C* we associate with the prominent peak in the bulk DOS occurring at 48.8 meV, while we associate the observed 44.8-meV mode with the very prominent TO peak in the bulk DOS occurring at 44.8 meV. In both of these cases, the peaks in the bulk DOS do not correspond to phonons at or near critical points in the Brillouin zone, but rather are associated with phonons in the interior of the zone. Finally, with regard to defect modes in the optical branch, we note that the present theory neglects defect-induced electrostatic interactions, and such effects are known to cause vibrational modes split off from the LO branch.[16]

We now come to the entry in Table I labeled Zn-O. This 6.0-meV mode is just barely resolved in the NN Zn-O pair spectrum of Henry, Dean, and Cuthbert[17] (a related mode[14] is seen at 9.2 meV for 2NN Zn-O pairs). Although the computational results presented here apply to the isolated O defect, simply replacing a NN Ga with a Zn atom changes the phonon energies by less than 0.1 meV since Ga and Zn have almost the same mass. Further force-constant variations of the Zn-O, Zn-P, or Zn-Ga interactions could affect the mode energies, but we assume that these variations are not significant. The presence of the Zn atom will, however, drastically affect the selection rules for observing phonons. In particular, all

modes which are T_2 for isolated O are now split to $A_1 \oplus E$, and strong phonon replicas of the allowed electronic transition transform as A_1. Thus, the low-energy T_2 mode in Fig. 5 should appear in the Zn-O spectrum, and we identify it with the observed 6.0-meV mode. The theoretical "eigenvector" for this mode is shown in Fig. 6. We plot the displacement eigenvector, $u = \underline{M}^{-1/2}\xi$, satisfying the eigenvalue equation

$$[\mathbb{1} - \underline{G}^0(\omega^2)\delta\underline{L}(\omega^2)]\xi = \lambda(\omega^2)\xi \tag{19}$$

at the resonant frequency, $\hbar\omega = 7.3$ meV, for which $\mathrm{Re}\lambda = 0$.[18] Now, the actual defect normal mode, given by $(\mathbb{1} - \underline{G}^0\delta\underline{L})\xi = 0$, requires a complex value of ω for its solution. However, since $\mathrm{Im}\lambda$ is proportional to the resonance width, we expect, for the very sharp 7.3-meV mode, that ω is near the real axis so that Eq. (19) gives a reasonable representation of the atomic motion in this case. It has been argued that this particular resonant mode plays an essential role in the dissociation of Zn-O pairs.[14] In particular, the atomic motions which occur during the early stages of the dissociation may be as shown in Fig. 6. It is seen that the amplitude of Zn-atom motion is roughly 3 times that of oxygen. Thus, we conclude that in the pair dissociation it is the Zn atom which jumps to an interstitial site and diffuses away.

The vibrational modes of NN Cd-O pairs have been observed in optical spectra,[17,19,20] and can be qualitatively understood on the basis of our calculations. The Cd-O modes will be similar to the Zn-O modes, except that those vibrations involving significant Cd motion will be shifted down in energy. Replicas of the electronically allowed A line should have A_1 symmetry for the point group C_{3v}, i.e., the A_1 modes and the A_1 component of the T_2 modes for isolated oxygen.[19] In emission, Henry, Dean, Thomas, and Hopfield observe local modes at 7.0, 47.3, and 49.7 meV.[20] The 7.0-meV mode is similar to the 6.0-meV Zn-O mode discussed above. Thus, this mode involves mainly Cd motion in agreement with the observed isotope shift.[17] The optical resonances at 47.3 and 49.7 meV are probably associated with the defect B and a_1(P) modes, thus involving mainly P-shell motion. From the intensities of the observed phonon replicas we conclude that in the optical transition the major atomic motion is that of the Cd atom moving relative to the almost stationary O atom. A number of Γ_3 phonons are reported[20] which produce replicas of the forbidden B line. Theoretically, we expect these to arise from the E modes and the E components of the T_1 and T_2 modes for isolated oxygen. As shown in Table I we do compute various E and T_1 modes. All these modes are very sharp (width of ~ 0.1 meV) and are tied to singularities in the bulk DOS. These modes could account for some of the observed Γ_3 modes, and the E components of the T_2 mode at 43.1 meV may also contribute. Our optical-phonon energies really are not accurate enough to make a definitive identification of these observed Γ_3 phonons.

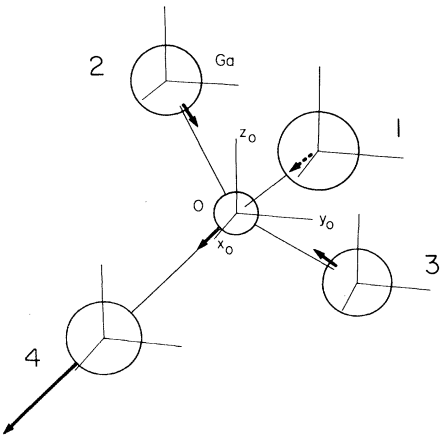

FIG. 6. "Eigenvector" for the 7.3-meV T_2 mode. The atomic displacements are indicated for the O and its four Ga neighbors. The $Ga_{(4)}$ and O displacements (in the ratio 3.4:1) both lie along the bond direction. The eigenvector has C_{3v} symmetry relative to the O—$Ga_{(4)}$ bond. With Zn in place of the $Ga_{(4)}$ atom, this is the predominant motion involved in the dissociation of Zn-O pairs (see text).

Let us consider what our calculations tell us about the nature of the oxygen defect. In particular, two opposing models[21,22] presently exist for this defect, and it is desirable to try to choose between them based on our results. First, the defect we are considering in our calculations is only a model, without the same detailed properties of the actual oxygen defect although their general properties should be similar. The most important result from our calculations is the O-lattice effective force constant, 3.5 eV/Å^2. This number is accurate to within, perhaps, 10%, and so provides a test of the opposing models. Unfortunately, it is very difficult to accurately obtain the defect force constant from the existing theoretical models. To date, Baraff *et al.*[15] have attempted such a calculation for the classical model[6,22] and have obtained an O-Ga stretching constant of 4.4 eV/Å^2, corresponding to an effective force constant of $4(4.4)/3 = 5.9$ eV/Å^2, a result which is somewhat too large. Nobody has yet attempted a similar computation for the weak-bonding model,[21] although the computed bond strength should be significantly different for the two models as they contain different numbers of bonding and antibonding electrons.[23] Morgan has recently argued that the observed structure near 25 meV in the O^0 phonon sidebands is due to a dynamic Jahn-Teller distortion of the O^0 defect.[23] Although such a distortion could occur, our calculations demonstrate that it is not necessary to invoke this mechanism in order to account for the observed structure. With one free parameter (η), we have obtained quantitative agreement between experiment and theory for those phonon energies, isotope shifts, and intensities.

One basis for the weak-bonding model[21] is the 19-meV a_1(Ga) phonon, present in donor-acceptor—pair (DAP) spectra,[1,3] but apparently absent in photoluminescence-excitation (PLE) spectra.[2] According to our calculations, this mode is rather broad as seen in the Ga-shell A_1 LDOS for O on a P site, shown in Fig. 4. Clearly, this resonance is distributed throughout the acoustic branch, so let us take its "width" to be 5 meV. This width has no consequence in the DAP spectrum due to the greater-than-10-meV broadening caused by a distribution of pair separations. But in the PLE spectrum, the no-phonon line is relatively sharp, so that the ratio of peak heights be-

tween an a_1(Ga)-phonon—assisted line and a no-phonon line is significantly reduced from the DAP spectrum. Additional broadening for the phonon-assisted line is also possible; the 20.4-meV Ga-shell peak in the A_1 LDOS for O on a P site shown in Fig. 4 represents mainly NN Ga motion. Motion of further-lying Ga shells will be concentrated at energies closer to 27 meV, and the actual phonon sideband probably involves some combination of these motions. We feel that a calculation of these broadening effects would be useful in order to quantify the apparent "anomaly."[21]

V. CONCLUSION

The major results of this paper are concerned with the existence of defect vibrational modes, including both strictly localized and resonant modes. It is impossible to determine the number of such modes by group theory alone since the existence of a mode is determined by a quantitative parameter: the degree of localization around the defect. Thus, it is necessary to undertake a computation of the vibrational modes of a defect. The theory we use for this purpose is a phenomenological one in which the force constants of the perfect lattice and those of the defect are all chosen to match experiment. Bulk phonons are described by a 15-parameter model which includes NN and 2NN plus electrostatic interactions. A defect is then introduced by perturbing the mass of an atom and perturbing its NN and 2NN force constants. A Green's-function technique is used to evaluate the LDOS near the defect, and thereby determine the presence of defect modes.

Our theoretical results are compared with experiment for the GaP:O_P defect. We use a two-parameter description of the short-range interaction perturbation near the O site. By a suitable choice of these two defect force constants we have obtained quantitative agreement with observed phonon modes involving O^+ and O^0 defects. For O-neighbor (i.e., O-Ga and O-P) and Ga-P (back-bond) short-range defect force constants at 38% and 93% of their respective bulk values, our calculations predict two A_1 modes and two T_2 modes which are reasonably localized at or near the defect, and also, other modes which are more bulklike in nature. We summarize the character of the four most localized modes as follows.

(1) *O-atom T_2 mode.* This mode involves mainly O-atom motion, and this motion is localized near the defect for practically any value of the defect force constants. To match the observed phonon energies near 25 meV, our choice of defect force constants correspond to an O-lattice effective force constant (taking all long-range and short-range interactions into account) of 3.5 eV/Å^2, which is 25% of the bulk, P-lattice value. This force constant may be compared with that obtained by assuming that the observed phonon is completely localized on the oxygen impurity, $(25\ \text{meV}/\hbar)^2 m_O = 2.4\ \text{eV/Å}^2$. Our calculations demonstrate that the observed two-peak structure in this resonant mode is due to coupling with LA bulk phonons.

(2) *Ga-shell T_2 mode.* This mode involves mainly vectorlike motion of the shell of Ga atoms surrounding the O impurity. The mode originates from the TA peak in bulk-phonon DOS, and is significantly localized around the defect for values of the O-neighbor force constants which are about 80% or less of the bulk values. Experimentally, this mode is not seen in spectra involving isolated O impurities, but is seen when a Zn or Cd atom is located near the O atom, thereby lowering the symmetry of the system.

(3) *Ga-shell A_1 mode.* This mode is a breathing motion of the Ga shell. The mode originates at the peak in the LA bulk-phonon DOS and is localized for values of the O-neighbor force constants which are about 80% or less of the bulk values. This resonant mode is relatively broad with a width of about 5 meV (in agreement with experiment).

(4) *P-shell A_1 mode.* This mode mainly involves breathing motion of the P shell (2NN's) surrounding the O atom. The mode originates at the LO peak in the bulk DOS, and appears when the Ga-P back-bond interactions are reduced to 95% or less of the bulk values.

For all of the four defect modes discussed above, we feel that our theoretical description is fairly close to experiment in terms of energies and eigenvectors. We have demonstrated that the O^+ and O^0 defects are weakly bound in GaP, as expected, and that the Ga—P back bonds appear to be weakened. Our predicted two-peak, O-atom T_2 mode shows that the experimental results for the O^0 defect are consistent with a T_d-symmetric geometry. Finally, our calculations identify the predominant atomic motion involved in the dissociation of Zn-O pairs in GaP.

ACKNOWLEDGMENTS

We gratefully acknowledge the support of the Office of Naval Research under Contract No. N00014-81K-0305. One of us (R.M.F.) has profited from the insights of T. N. Morgan.

APPENDIX

We have determined the collective coordinates Q for the 12-atom, 2NN shell seen by a substitutional defect in a zinc-blende lattice. The collective coordinates form bases for the irreducible representations of the symmetry group of the 2NN shell, namely O_h. The equilibrium positions of the 12 atoms in the 2NN shell are given (in units of $a_0/2$) by

$$\begin{aligned} &\vec{r}_1 = -\vec{r}_7 = (0,1,1)\ , \quad \vec{r}_2 = -\vec{r}_8 = (1,0,1)\ , \\ &\vec{r}_3 = -\vec{r}_9 = (1,1,0)\ , \quad \vec{r}_4 = -\vec{r}_{10} = (-1,1,0)\ , \\ &\vec{r}_5 = -\vec{r}_{11} = (0,-1,1)\ , \quad \vec{r}_6 = -\vec{r}_{12} = (1,0,-1)\ , \end{aligned} \tag{A1}$$

where a_0 is the edge length of the conventional unit cell. The 36 collective coordinates Q are related by an orthogonal transformation to the 36 Cartesian displacements, (x_i, y_i, z_i), of atom i from equilibrium, where $i = 1, \ldots, 12$. The explicit form of this orthogonal transformation is given in Table II. In this work, the

TABLE II. 36 collective coordinates Q for the 12-atom, 2NN shell. The (unnormalized) components associated with the atoms $i=1,\ldots,6$ are given explicitly. The components associated with the remaining atoms ($i=7,\ldots,12$) are obtained by multiplying the entire row of coefficients by the sign indicated. The irreducible representation of the T_d group according to which the collective coordinates transform are also indicated.

Q	(s)	x_1	y_1	z_1	x_2	y_2	z_2	x_3	y_3	z_3	x_4	y_4	z_4	x_5	y_5	z_5	x_6	z_6	z_6	(+ or −)
Q_1	A_1	0	1	1	1	0	1	1	1	0	$\bar{1}$	1	0	0	$\bar{1}$	1	1	0	$\bar{1}$	−
Q_2	A_1	1	0	0	0	1	0	0	0	1	0	0	$\bar{1}$	$\bar{1}$	0	0	0	$\bar{1}$	0	+
Q_3	A_2	0	$\bar{1}$	1	1	0	$\bar{1}$	$\bar{1}$	1	0	1	1	0	0	1	1	1	0	1	−
Q_4	E	0	1	1	1	0	1	$\bar{2}$	$\bar{2}$	0	2	$\bar{2}$	0	0	$\bar{1}$	1	1	0	$\bar{1}$	−
Q_5	E	0	$\bar{1}$	$\bar{1}$	1	0	1	0	0	0	0	0	0	0	1	$\bar{1}$	1	0	$\bar{1}$	−
Q_6	E	0	$\bar{1}$	1	$\bar{1}$	0	1	0	0	0	0	0	0	0	1	1	$\bar{1}$	0	$\bar{1}$	−
Q_7	E	0	$\bar{1}$	1	1	0	$\bar{1}$	2	$\bar{2}$	0	$\bar{2}$	$\bar{2}$	0	0	1	1	1	0	1	−
Q_8	E	1	0	0	0	1	0	0	0	$\bar{2}$	0	0	2	$\bar{1}$	0	0	0	$\bar{1}$	0	+
Q_9	E	$\bar{1}$	0	0	0	1	0	0	0	0	0	0	0	1	0	0	0	$\bar{1}$	0	+
Q_{10}	T_1	0	0	0	0	$\bar{1}$	0	0	0	1	0	0	1	0	0	0	0	1	0	−
Q_{11}	T_1	1	0	0	0	0	0	0	0	$\bar{1}$	0	0	1	1	0	0	0	0	0	−
Q_{12}	T_1	$\bar{1}$	0	0	0	1	0	0	0	0	0	0	0	1	0	0	0	1	0	−
Q_{13}	T_1	0	$\bar{1}$	1	0	0	0	0	0	0	0	0	0	0	$\bar{1}$	$\bar{1}$	0	0	0	−
Q_{14}	T_1	0	0	0	1	0	$\bar{1}$	0	0	0	0	0	0	0	0	0	$\bar{1}$	0	$\bar{1}$	−
Q_{15}	T_1	0	0	0	0	0	0	$\bar{1}$	1	0	$\bar{1}$	$\bar{1}$	0	0	0	0	0	0	0	−
Q_{16}	T_1	0	0	0	1	0	$\bar{1}$	$\bar{1}$	1	0	$\bar{1}$	$\bar{1}$	0	0	0	0	1	0	1	+
Q_{17}	T_1	0	$\bar{1}$	1	0	0	0	$\bar{1}$	1	0	1	1	0	0	$\bar{1}$	$\bar{1}$	0	0	0	+
Q_{18}	T_1	0	$\bar{1}$	1	1	0	$\bar{1}$	0	0	0	0	0	0	0	1	1	$\bar{1}$	0	$\bar{1}$	+
Q_{19}	T_1	0	0	0	$\bar{1}$	0	$\bar{1}$	1	1	0	1	$\bar{1}$	0	0	0	0	$\bar{1}$	0	1	+
Q_{20}	T_1	0	1	1	0	0	0	$\bar{1}$	$\bar{1}$	0	1	$\bar{1}$	0	0	1	$\bar{1}$	0	0	0	+
Q_{21}	T_1	0	$\bar{1}$	$\bar{1}$	1	0	1	0	0	0	0	0	0	0	1	$\bar{1}$	$\bar{1}$	0	1	+
Q_{22}	T_2	0	0	0	1	0	1	1	1	0	1	$\bar{1}$	0	0	0	0	1	0	$\bar{1}$	+
Q_{23}	T_2	0	1	1	0	0	0	1	1	0	$\bar{1}$	1	0	0	1	$\bar{1}$	0	0	0	+
Q_{24}	T_2	0	1	1	1	0	1	0	0	0	0	0	0	0	$\bar{1}$	1	$\bar{1}$	0	1	+
Q_{25}	T_2	1	0	0	0	0	0	0	0	0	0	0	0	1	0	0	0	0	0	+
Q_{26}	T_2	0	0	0	0	1	0	0	0	0	0	0	0	0	0	0	0	1	0	+
Q_{27}	T_2	0	0	0	0	0	0	0	0	1	0	0	1	0	0	0	0	0	0	+
Q_{28}	T_2	0	0	0	1	0	$\bar{1}$	1	$\bar{1}$	0	1	1	0	0	0	0	1	0	1	+
Q_{29}	T_2	0	1	$\bar{1}$	0	0	0	$\bar{1}$	1	0	1	1	0	0	1	1	0	0	0	+
Q_{30}	T_2	0	$\bar{1}$	1	$\bar{1}$	0	1	0	0	0	0	0	0	0	1	1	1	0	1	+
Q_{31}	T_2	0	0	0	0	$\bar{1}$	0	0	0	$\bar{1}$	0	0	$\bar{1}$	0	0	0	0	1	0	−
Q_{32}	T_2	$\bar{1}$	0	0	0	0	0	0	0	$\bar{1}$	0	0	1	$\bar{1}$	0	0	0	0	0	−
Q_{33}	T_2	$\bar{1}$	0	0	0	$\bar{1}$	0	0	0	0	0	0	0	1	0	0	0	$\bar{1}$	0	−
Q_{34}	T_2	0	1	1	0	0	0	0	0	0	0	0	0	0	1	$\bar{1}$	0	0	0	−
Q_{35}	T_2	0	0	0	1	0	1	0	0	0	0	0	0	0	0	0	$\bar{1}$	0	1	−
Q_{36}	T_2	0	0	0	0	0	0	1	1	0	1	$\bar{1}$	0	0	0	0	0	0	0	−

symmetry of the defect is T_d. Accordingly, the collective coordinates presented here form bases for the irreducible representations of the T_d as well as the O_h point groups. The T_d representations associated with various Q's are indicated in Table II. The corresponding O_h representations may be obtained from Table II with the substitutions, $A_1^- \rightarrow A_{1g}$, $A_1^+ \rightarrow A_{2u}$, $A_2^- \rightarrow A_{2g}$, $E^- \rightarrow E_g$, $E^+ \rightarrow E_u$, $T_1^- \rightarrow T_{1g}$, $T_1^+ \rightarrow T_{2u}$, $T_2^- \rightarrow T_{2g}$, and $T_2^+ \rightarrow T_{1u}$, where the plus or minus sign superscript refers to the rightmost column entry in the table.

[1] P. J. Dean, C. H. Henry, and C. J. Frosch, Phys. Rev. 168, 812 (1968).

[2] P. J. Dean and C. H. Henry, Phys. Rev. 176, 928 (1968).

[3] B. Monemar and L. Samuelson, J. Lumin. 12-13, 507 (1976); Phys. Rev. B 18, 809 (1978).

[4] T. N. Morgan, Phys. Rev. Lett. 40, 190 (1968).

[5] G. A. Baraff, E. O. Kane, and M. Schlüter, Phys. Rev. Lett. 47, 601 (1981).

[6] P. J. Dean, Physica 178&118B, 140 (1983).

[7] R. M. Feenstra, R. J. Hauenstein, and T. C. McGill, Phys. Rev. B 28, 5793 (1983).

[8] K. Kunc and M. Balkanski, Phys. Rev. B 12, 4346 (1975); K. Kunc, M. Balkanski, and M. A. Nusimovici, Phys. Status Solidi B 71, 341 (1975); 72, 229 (1975); 72, 249 (1975).

[9] A. A. Maradudin, E. W. Montroll, G. H. Weiss, and I. P. Ipatova, in *Solid State Physics*, 2nd ed., edited by H. Ehrenreich, F. Seitz, and D. Turnbull (Academic, New York, 1971), Suppl. 3, Chap. 2.

[10] In *Solid State Physics*, Ref. 9, Chap. 8.

[11] P. J. Dean, Phys. Rev. 157, 655 (1967).

[12] K. K. Rebane, *Impurity Spectra of Solids* (Plenum, New York, 1970).

[13]G. Herzberg, *Molecular Spectra and Molecular Structure* (Van Nostrand and Reinhold, New York, 1966), Vol. III.

[14]R. M. Feenstra and T. C. McGill, Phys. Rev. Lett. 47, 925 (1981).

[15]G. Baraff, E. O. Kane, and M. Schlüter, Phys. Rev. B 25, 548 (1982).

[16]P. J. Dean, D. D. Manchon, Jr., and J. J. Hopfield, Phys. Rev. Lett. 25, 1027 (1970).

[17]C. H. Henry, P. J. Dean, and J. D. Cuthbert, Phys. Rev. 166, 754 (1968).

[18]The condition, $\mathrm{Re}\lambda = 0$, is an alternative to Eq. (9) for identifying resonant modes. (See *Solid State Physics,* Ref. 9, pp. 386ff.)

[19]T. N. Morgan, B. Welber, and R. N. Bhargava, Phys. Rev. 166, 751 (1968).

[20]C. H. Henry, P. J. Dean, D. G. Thomas, and J. J. Hopfield, in *Localized Excitations in Solids,* edited by R. F. Wallis (Plenum, New York, 1968), p. 267.

[21]T. N. Morgan, Phys. Rev. Lett. 49, 173 (1982); Physica 117&118B, 146 (1983).

[22]P. J. Dean, M. S. Skolnick, Ch. Uihlein, and D. C. Herbert, J. Phys. C 16, 2017 (1983).

[23]T. N. Morgan, Phys. Rev. B 28, 6107 (1983).